# Supporting Information

## Self-assembled VN/$Ti_3C_2T_x$ composites for asymmetric supercapacitors

Di Wang [1], Deyang Zhang [1*], Binhe Feng [1], Jinbing Cheng [2*], Zuxue Bai [1], Zhaorui Wang [1], Jin Chang [1, 3], Paul K. Chu [4], Yang Lu [1*], Yongsong Luo [1, 2*]

[1] *Key Laboratory of Microelectronics and Energy of Henan Province, Engineering Research Center for MXene Energy Storage Materials of Henan Province, Henan Joint International Research Laboratory of New Energy Storage Technology, Xinyang Normal University, Xinyang 464000, P. R. China*

[2] *Henan International Joint Laboratory of MXene Materials Microstructure, College of Physics and Electronic Engineering, Nanyang Normal University, Nanyang 473061, P. R. China*

[3] *PingDingShan University，PingDingShan 467000, P. R. China*

[4] *Department of Physics, Department of Materials Science & Engineering, and Department of Biomedical Engineering, City University of Hong Kong, Tat Chee Avenue, Kowloon, Hong Kong, China*

* Corresponding author. Tel./fax: +86 376 6391760, E-mail: zdy@xynu.edu.cn (D. Y. Zhang), chengjinbing1988@163.com, luyang.181@163.com (Y. Lu), ysluo@xynu.edu.cn (Y. S. Luo).

# 1 Experimental section

## 1.1 Materials characterization

Powder X-ray diffraction (XRD) (Rigaku Smartlab 9 kW Japan) was performed at 45 kV and 200 mA with Cu K$\alpha$ radiation ($\lambda$ = 1.5406 Å). The morphology was observed on the Hitachi S-4800 scanning electron microscope and FEI Tecnai G2 F20 transmission electron microscope (TEM) at 200 kV. X-ray photoelectron spectroscopy (XPS) was carried out on the K-Alpha+ (Thermo Scientific) with a 50 eV pass energy and 1.0 eV energy step. The elemental analysis was conducted on the energy-dispersive X-ray spectrometer (HAADF-STEM-EDS).

## 1.2 Electrochemical measurements

The electrochemical properties of VN, $Ti_3C_2T_x$, and $Ti_3C_2T_x$/VN were determined in 3 M KOH on the CHI660E electrochemical workstation using the traditional three-electrode configuration at 25 °C with platinum and Hg/HgO as the counter and reference electrodes, respectively. The working electrode was prepared by mixing the active materials, conductive carbon black, and polytetrafluoroethylene (PTFE) emulsion with a mass ratio of 8:1:1. An appropriate amount of anhydrous ethanol was added to the mixture and stirred. The slurry was coated on a 1×1 $cm^2$ nickel foam substrate and dried for 12 hours. Cyclic voltammetry (CV) and galvanostatic charging-discharging (GCD) were performed at various scanning rates to gauge the rate capability of the active electrode. Electrochemical impedance spectroscopy (EIS) was

conducted in a frequency region of 100 kHz to 0.01 Hz at an open circuit potential of 10 mV. The specific capacitance ($C_m$, F $g^{-1}$) was calculated as follows:

$$C_m = \frac{I \times \Delta t}{m \times \Delta V} \quad (1)$$

where I (A) is the applied current, $\Delta t$(s) is the discharging time, $\Delta V$ (V) is the disch arging potential range, and m (g) is the total mass of active materials, respectively. The theoretical pseudocapacitance was calculated as follows:

$$C = \frac{n \times F}{M \times V} \quad (2)$$

where n (mol) is the number of electrons transferred in the redox reaction, M (g. $mol^{-1}$) is the molar mass of the materials, and F (C. $mol^{-1}$) is Faraday's constant and V (V) is the operating voltage window, respectively.

The asymmetric supercapacitor device was assembled by $Ti_3C_2T_x$/VN as the positive electrode and AC as the negative electrode. In order to obtain the best electrochemical characteristics of $Co_3O_4$// $Ti_3C_2T_x$ /VN, the charge balance between the two electrodes follows the relationship of q+ = q-, where q is the charge stored by the electrode calculated by the following equation:

$$q = C_m \times \Delta E \times m \quad (3)$$

where Cm (F $g^{-1}$) is the specific capacitance, ΔE (V) is the potential range of the charging/discharging process, and m (g) is the mass loading of the active materials. According to equation (3), the ideal mass ratio of the active materials on the positive ($Ti_3C_2T_x$/VN) to that on the negative electrode ($Co_3O_4$) ($m^+/m^-$) can be calculated by the following:

$$\frac{m_+}{m_-} = \frac{\Delta E_- \times C_-}{\Delta E_+ \times C_+} \quad (4)$$

The energy density (E) and power density (P) can be calculated by the following equations:

$$E = \frac{1}{2} C_m (\Delta V)^2 \quad (5)$$

and

$$P = \frac{E}{\Delta t} \quad (6)$$

where E (Wh $kg^{-1}$) is the energy density, m (F $g^{-1}$) is the specific capacitance, ΔV (V) is the operating potential window, P (kW $kg^{-1}$) is the power density, and Δt(s) is the discharging time.

To study the charge storage mechanisms, the following equation is adopted to define the capacitive capacitance in the total capacitance:

$$I(V) = k_1 V + k_2 V^{1/2}. \quad (7)$$

The first term on the right side of the equation corresponds to the capacitance-controlled effect and the other involves diffusion-controlled insertion. i(V) and v are the current at potential V and scanning rate, slope, and intercept by plotting $i(V)/v^{1/2}$ against $v^{1/2}$.

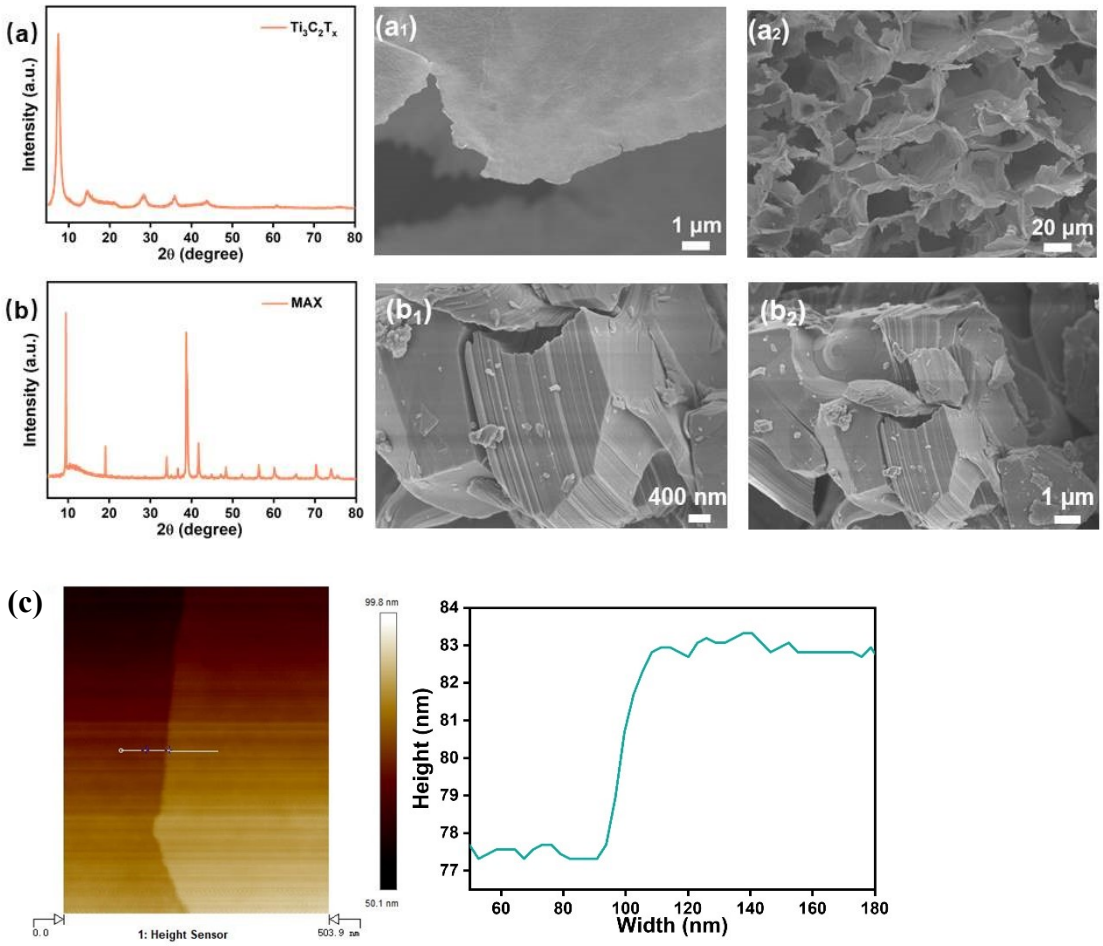


**Figure S1.** (a) XRD pattern of $Ti_3C_2T_x$, SEM images of ($a_1$, $a_2$); (b) XRD pattern of MAX, SEM images of ($b_1$, $b_2$); (c) the $Ti_3C_2T_x$ nanosheet.

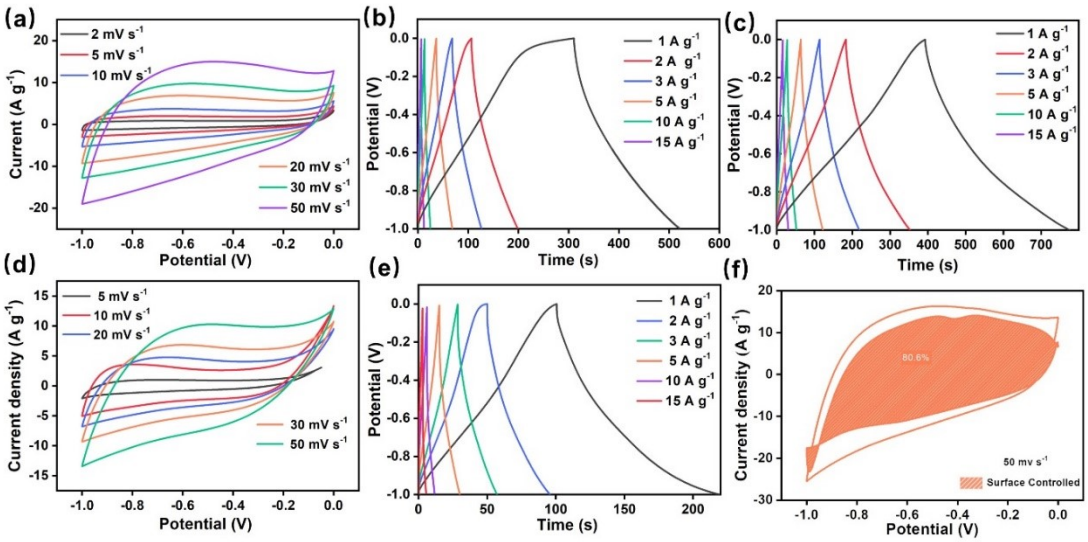


**Figure S2.** (a) CV and (b) GCD curves of the VN electrolyte at various scan rates (2–50 mV $s^{-1}$) and various current densities (1–15 A $g^{-1}$). (c)GCD curves of $Ti_3C_2T_x$/VN for different current densities. (d) CV and (e) GCD curves of the $Ti_3C_2T_x$ electrolyte. (f) Capacitive contribution at a scan rate of 50 mV $s^{-1}$.

| Materials | Specific capacitance (F $g^{-1}$) | Potential window/ V | Cycle number (%) | Reference |
|---|---|---|---|---|
| **$Ti_3C_2T_x$/VN** | 382.1 | 1 | 5000/93.5% | This Work |
| **VN/NG** | 370 | 1.2 | 10000/98.66% | Ref [1] |
| CNS@VN | 300.4 | 1 | 5000/70.8% | Ref [2] |
| VN/NCS | 148 | 1 | 5000/78% | Ref [3] |
| **VN/PEDOT** | 226.2 | 1 | 5000/91.5% | Ref [4] |
| **VN/NPC** | 198.3 | 1 | 16000/107.6% | Ref [5] |

**Table S1.** Comparison of the electrochemical properties of different electrodes based on VN.

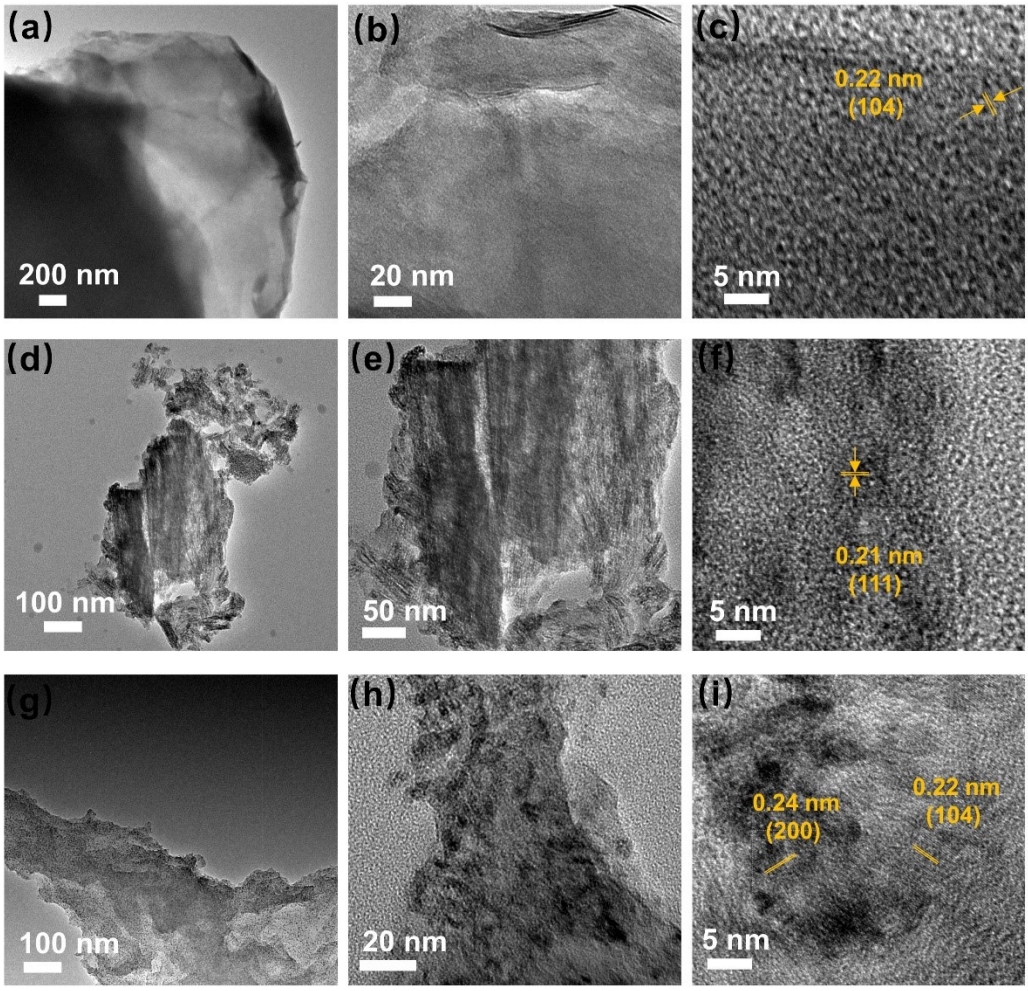


**Figure S3.** TEM and HR-TEM images of (a-c) $Ti_3C_2T_x$, (d-f) VN, (g-i) $Ti_3C_2T_x$/VN after cycling.

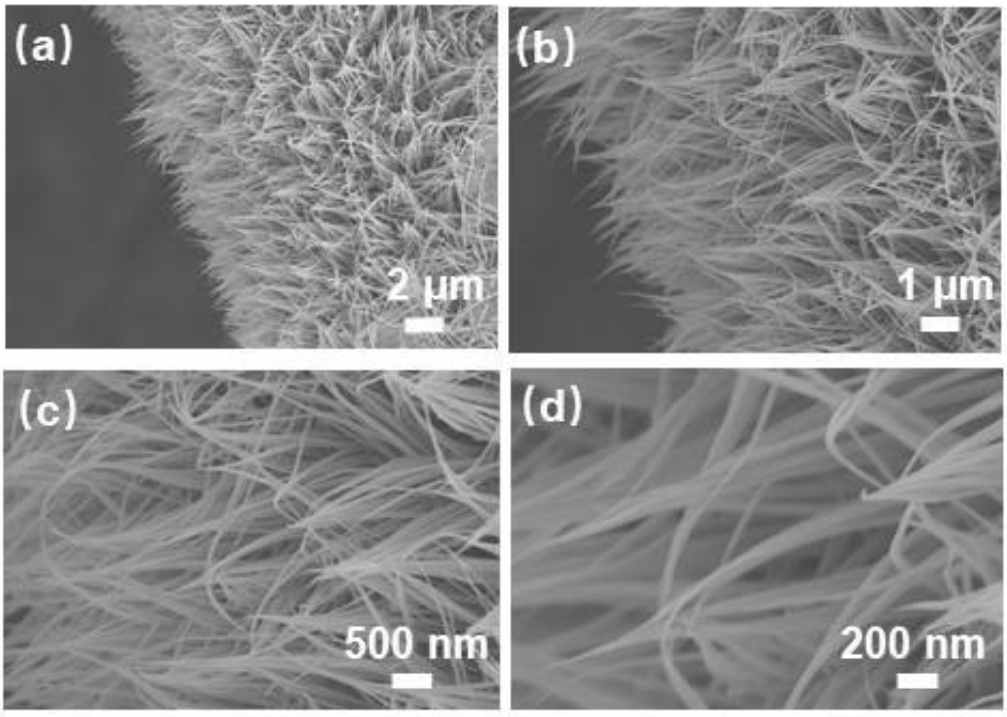


**Figure S4.** SEM images of the $Co_3O_4$ electrode.

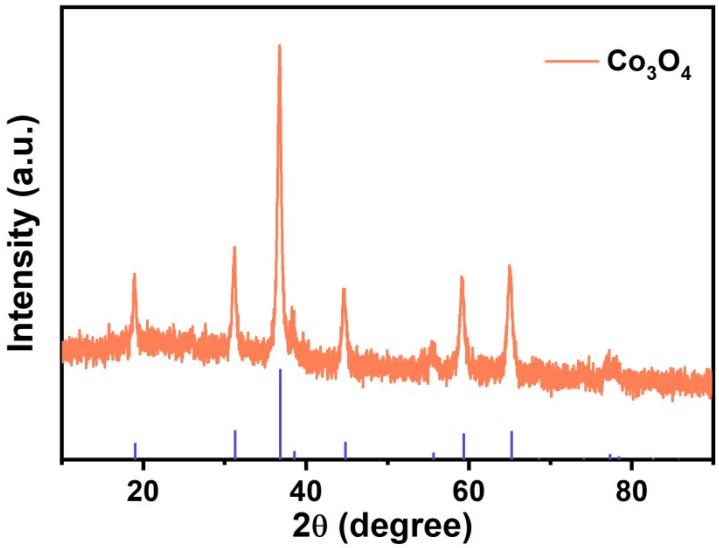


**Figure S5.** XRD pattern of $Co_3O_4$.

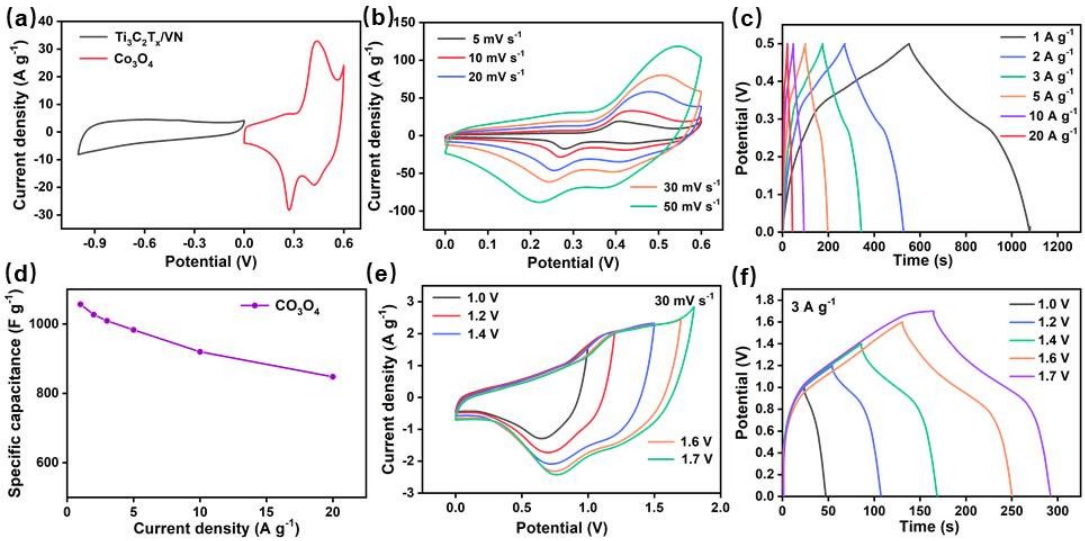


**Figure S6.** (a) CV curves of $Ti_3C_2T_x$/VN and $Co_3O_4$; (b, c) CV curves and GCD plots of $Co_3O_4$ (d) Specific capacities of $Co_3O_4$; (e) CV curves acquired at a scanning rate of 30 mV $s^{-1}$ in different voltage windows; (f) GCD curves acquired at 3 A $g^{-1}$ in different voltage windows.

**Table S2.** Comparison of the electrochemical properties of different electrodes based on VN.

| Materials | Potential window (V) | Energy densities (Wh $kg^{-1}$) | Power densities (W $kg^{-1}$) | Cycle number | References |
|---|---|---|---|---|---|
| $Co_3O_4$//$Ti_3C_2T_x$ /VN | (0-1.6) | 69.1 | 800 | 3000/91.9% | This Work |
| Co $(OH)_2$//VN | (0-1.6) | 22 | 160 | 4000> 80% | Ref [6] |
| NCA//VN/PEDOT | (0-1.6) | 48.36 | 1600 | 10000/91.6% | Ref [4] |
| MnO2@CC//VN-NWs@CC | (0.5-1.6) | 57.9 | 261.5 | 12000/118% | Ref [7] |
| $Co_3O_4$//CNS@VN | (0-1.6) | 18.8 | 800 | / | Ref [8] |
| PCNS@VNNP //NiO | (0-1.6) | 47.2 | 800 | 2500/97.5% | Ref [9] |
| VNQD/PC//Ni $(OH)_2$ | (0-1.6) | 31.2 | 780 | / | Ref [10] |
| HPCF@VNNP //Ni $(OH)_2$ | (0-1.6) | 39.3 | 400 | / | Ref [11] |
| $V_2O_3$/C//VN/NCS | (0-1.6) | 19.8 | 800 | / | Ref [12] |
| 0.04-VN/NCS-2//$NiCo_2S_4$ | (0-1.6) | 21 | 800 | / | Ref [13] |

| Materials | Potential window (V) | Energy densities | Power densities | Cycle number | References |
|---|---|---|---|---|---|
| **$Fe_2O_3$@VN/CC //$RuO_2$/CC** | 0-1.4V | 0.5 mWh $cm^{-2}$ | 12.28 mW $cm^{-2}$ | 15000/80% | Ref [14] |
| **ZNCO/NF//VN /CC** | 0-1.6V | 0.185 mWh $cm^{-2}$ | 22.4 mW $cm^{-2}$ | 8000/87% | Ref [15] |
| **VN/NPC// VN/NPC SSC** | 0-1V | 21.97 μWh $cm^{-2}$ | 0.5 mW $cm^{-2}$ | 18000/90.9 % | Ref [5] |

## References

[1] J. Balamurugan, G. Karthikeyan, T.D. Thanh, N.H. Kim, J.H. Lee, Facile synthesis

of vanadium nitride/nitrogen-doped graphene composite as stable high performance anode materials for supercapacitors, *J. Power Sources* 308 (2016) 149-157.
[2] Y. Liu, L. Liu, Y. Tan, L. Niu, L. Kong, L. Kang, F. Ran, Carbon nanosphere@vanadium nitride electrode materials derived from metal-organic nanospheres self-assembled by NH4VO3, chitosan, and amphiphilic block copolymer, Electrochim. Acta 262 (2018) 66-73.
[3] X. Jiang, W. Lu, X. Yu, S. Song, Y. Xing, Fabrication of a vanadium nitride/N-doped carbon hollow nanosphere composite as an efficient electrode material for asymmetric supercapacitors, Nanoscale Adv. 2(9) (2020) 3865-3871.
[4] Coupling PEDOT on Mesoporous Vanadium Nitride Arrays for Advanced Flexible All-Solid-State Supercapacitors.
[5] Z. Wu, Q. Chen, C. Li, L. Zhu, Y. Huang, X. Zhu, X. Zhu, Y. Sun, Hydrogel-derived nitrogen-doped porous carbon framework with vanadium nitride decoration for supercapacitors with superior cycling performance, J. Mater. Sci. Technol. 155 (2023) 167-174.
[6] R. Wang, X. Yan, J. Lang, Z. Zheng, P. Zhang, A hybrid supercapacitor based on flower-like $Co(OH)_2$ and urchin-like VN electrode materials, *J. Mater. Chem. A* 2(32) (2014) 12724-12732.
[7] M. Ma, Z. Shi, Y. Li, Y. Yang, Y. Zhang, Y. Wu, H. Zhao, E. Xie, High-performance 3 V “water in salt” aqueous asymmetric supercapacitors based on VN nanowire electrodes, J. Mater. Chem. A 8(9) (2020) 4827-4835.
[8] Y. Liu, L. Liu, Y. Tan, L. Niu, L. Kong, L. Kang, F. Ran, Carbon nanosphere@vanadium nitride electrode materials derived from metal-organic nanospheres self-assembled by NH4VO3, chitosan, and amphiphilic block copolymer, Electrochim. Acta 262 (2018) 66-73.
[9] G. Wang, S. Hou, C. Yan, X. Zhang, W. Dong, Preparation of three-dimensional vanadium nitride porous nanoribbon/graphene composite as an efficient electrode material for supercapacitors, *J. Mater. Sci. Mater. Electron.* 29(15) (2018) 13118-13124.
[10] Y. Yang, K. Shen, Y. Liu, Y. Tan, X. Zhao, J. Wu, X. Niu, F. Ran, Novel Hybrid Nanoparticles of Vanadium Nitride/Porous Carbon as an Anode Material for Symmetrical Supercapacitor, Nano-Micro Lett.
9(1) (2016) 6.
[11] Y. Liu, L. Liu, Y. Tan, L. Kong, L. Kang, F. Ran, Well-Dispersed Vanadium Nitride on Porous Carbon Networks Derived from Block Copolymer of PAN-b-PDMC-b-PAN Absorbed with Ammonium Metavanadate for Energy Storage Application, *J. Phys. Chem. C.* 122(1) (2018) 143-149.
[12] X. Jiang, W. Lu, X. Yu, S. Song, Y. Xing, Fabrication of a vanadium nitride/N-doped carbon hollow nanosphere composite as an efficient electrode material for asymmetric supercapacitors, *Nanoscale Adv.* 2(9) (2020) 3865-3871.
[13] X. Jiang, W. Lu, Y. Li, Y. Yu, X. Zhou, X. Liu, Y. Xing, An Eco-Friendly Nitrogen Source for the Preparation of Vanadium Nitride/Nitrogen-Doped Carbon Nanocomposites for Supercapacitors, ChemElectroChem 6(13) (2019) 3445-3453.
[14] H. Zhou, M. Alam, Y. Wu, Y. Zeng, A.N. Gandi, J. Zheng, W. Zhu, Z. Wang, H.

Liang, Synergy of VN and Fe2O3 Enables High Performance Anodes for Asymmetric Supercapacitors, ACS Appl. Mater. Interfaces 15(15) (2023) 18819-18827.
[15] Z. Wu, H. Li, H. Li, B. Yang, R. Wei, X. Zhu, X. Zhu, Y. Sun, Direct growth of porous vanadium nitride on carbon cloth with commercial-level mass loading for solid-state supercapacitors, Chem. Eng. J. 444 (2022).